Catalytic Urea Electrooxidation on Nickel-Metal Hydroxide Foams For Use in A Simplified Dialysis Device

Anthony Pyka[1], David S. Bergsman[1], and Eric Stuve[1]

[1]University of Washington Department of Chemical Engineering

May 02, 2024

Abstract

Electrocatalytic urea removal is a promising technology for artificial kidney dialysis and wastewater treatment. Urea electrooxidation was studied on a variety of nickel electrocatalysts modified with Cr, Mo, Mn, and Fe with varying electrochemically active surface and roughness. Mass transfer limits were observed for urea oxidation at physiological concentrations (10 mM). Urea oxidation kinetics were explored at higher concentrations (200 mM), showing improved performance during polarization, but lower currents per active site. A simplified dialysis model was developed to examine the relationship of mass transfer coefficients and extent of reaction on flowrate, composition, and pH of the reacting stream. For a nickel hydroxide catalyst, the model shows that a minimum electrode area of 1314 cm ^{2} is needed for continuous operation. This research combines experimental data and a computational dialysis model for a simplified continuous dialysis system, highlighting the potential of these catalysts and paving the way for future improvements.

Catalytic Urea Electrooxidation on Nickel-Metal Hydroxide Foams For Use in A Simplified Dialysis Device

Anthony Pyka (0009-0006-8458-8316)[1,2], David S. Bergsman (0000-0002-0141-6417)[1,3], and Eric Stuve (0000-0003-4948-2314)[1,*]

[1]Department of Chemical Engineering, University of Washington, Seattle, WA, USA

[2]Contributing Author. pykachu6@uw.edu

[3]Contributing Author. dbergs@uw.edu

[*]Corresponding Author. stuve@uw.edu

March 13, 2024

Abstract

Electrocatalytic urea removal is a promising technology for artificial kidney dialysis and wastewater treatment. Urea electrooxidation was studied on a variety of nickel electrocatalysts modified with Cr, Mo, Mn, and Fe with varying electrochemically active surface and roughness. Mass transfer limits were observed for urea oxidation at physiological concentrations (10 mM). Urea oxidation kinetics were explored at higher concentrations (200 mM), showing improved performance

during polarization, but lower currents per active site. A simplified dialysis model was developed to examine the relationship of mass transfer coefficients and extent of reaction on flowrate, composition, and pH of the reacting stream. For a nickel hydroxide catalyst, the model shows that a minimum electrode area of 1314 cm^2 is needed for continuous operation. This research combines experimental data and a computational dialysis model for a simplified continuous dialysis system, highlighting the potential of these catalysts and paving the way for future improvements.

Topical Heading and Key Words

Topical Heading: Reaction Engineering, Kinetics and Catalysis

Key Words:

- Urea Electrooxidation
- Portable Dialysis
- Nickel Hydroxide Foam
- Nickel Electrode Electrocatalysts
- Electrochemically Active Surface Area

1 Introduction

Access to affordable chronic kidney disease treatment is a major problem since the increasing number of patients with end-stage kidney disease has outpaced the growth of available treatment options.[1] Patients diagnosed with end-stage renal failure suffer from high burdens and have high rates of mortality.[2] The high burden, coupled with co-morbidity and related mental issues like depression, lead to a poor health-related quality of life.[3–5] There is evidence suggesting more frequent treatments, like daily home dialysis, would benefit patients by improving metabolic parameters.[2] The introduction of more frequent dialysis treatments reduces the magnitude of swings in toxin levels in the blood stream, thereby improving the patient's overall health.

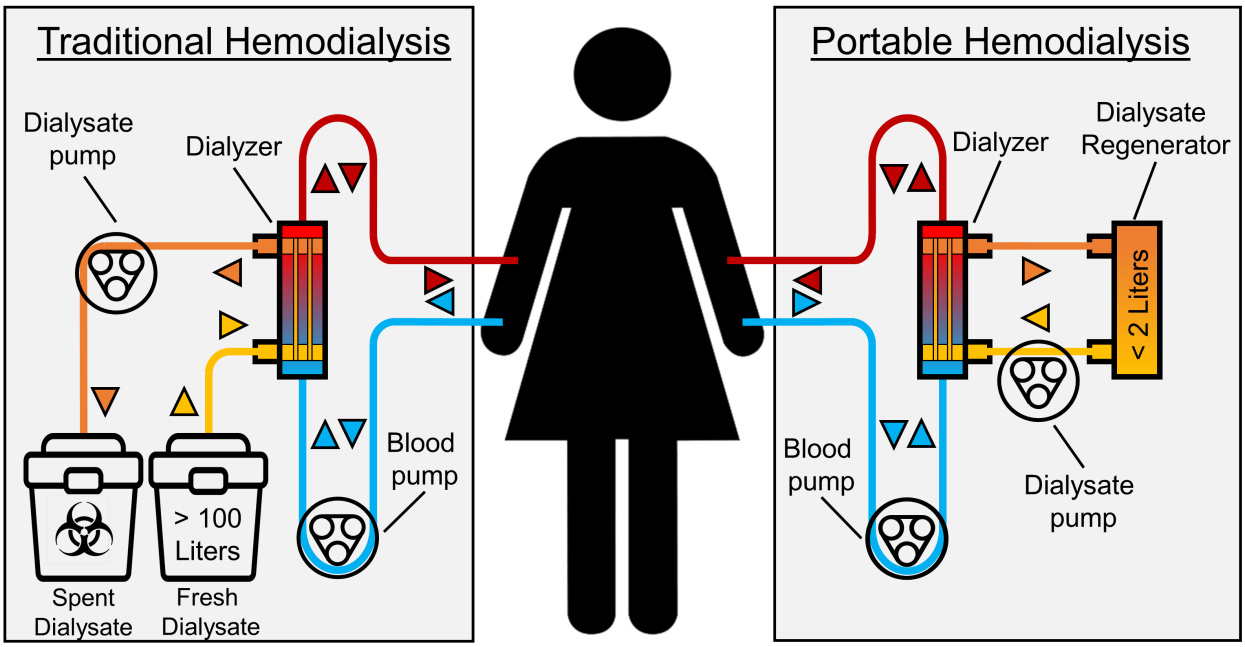

Figure 1: Depiction of traditional (left) and portable (right) hemodialysis. Traditional dialysis relies on a large amount of fresh dialysate composed of electrolytes and water to remove blood toxins in a single-pass configuration. Portable dialysis relies on a small amount of recycled dialysate to make the operation small enough to be comfortably carried.

The bottlenecks for converting patients from traditional dialysis to home dialysis are storage, cost, and disposal of dialysate. Traditional hemodialysis is an expensive process requiring 300-600 liters of dialysate per week.[6] The composition of the fresh dialysate is important as it influences the exchange of ions between the blood and the dialyzer, restores acid-base equilibrium, and strongly affects cardiovascular stability.[7] Patients of different ages, sizes, gender, and other external factors will have varying compositions of dialysate, making a "one size fits all" fluid difficult to achieve.[8]

One possible method to overcome the limitations of traditional dialysis is portable dialysis, as seen in Figure 1. Portable dialysis, employing a wearable artificial kidney (WAK), relies on a small amount of fluid customized to each individual and that does not need replacement. The dialysate regenerator in Fig. 1 needs to remove major waste components, such as urea, creatinine, peptides, and protein-bound toxins, in spent dialysate without appreciable loss of ions.[9] This study focuses solely on the removal of urea with a WAK, because urea is the species of highest concentration in spent dialysate.

The three major technologies for efficiently removing urea from spent dialysate are: physisorption and chemisorption, enzymatic hydrolysis, and reactive decomposition.[10] Physisorption and chemisorption with sorbent materials are ideal for a WAK as there are no byproducts of a reaction, but the sorbents are highly selective, requiring many different types to remove all uremic toxins.[11,12] Enzymatic hydrolysis utilizes urease to remove urea at near-neutral pH. The urea is converted to ammonium, which is far more toxic than urea; thus, extensive filters are required for implementation.[13]

Electrochemical removal, a form of reactive decomposition, for dialysate regeneration has been explored by several groups and has been shown to be an efficient method for urea removal for a WAK.[14–19] However, the method has never been applied in a clinical application with humans.[20–22] The reason a WAK has not been used in a clinical application has not been explicitly stated, but may be due to generation of chloride species, production of ammonia, overoxidation of urea into nitrite and nitrate species, or leaching of metal species.[20,23–26] Discovery of a catalyst that is stable and efficient, and produces safe reaction products is necessary for application.

Nickel is a promising anode material for electrochemical removal of urea in a WAK. Nickel, although susceptible to chloride corrosion, shows affinity for urea electrooxidation with low selectivity for ammonia-type compounds.[16,27–29] Addition of other metals into nickel have been shown to improve passivation and minimize corrosion, but their effect on urea oxidation activity has not been well understood.[30–33]

The urea oxidation reaction (UOR) is catalyzed by the presence of nickel oxyhydroxide (NiOOH), as seen by Reaction 1.[34,35] There is debate whether or not the nickel hydroxide sites are consumed during UOR, since UOR is mediated through the electrochemical activation of nickel from $Ni(OH)_2$ to NiOOH at 1.35 V_{RHE}, as seen by Reaction 2.[36,37] A catalyst regeneration mechanism (where $Ni(OH)_2$ is inactive and NiOOH is active) has been identified as the mechanism most relevant near the $Ni(OH)_2$/NiOOH onset potential and is adopted here:[38]

$$CO(NH_2)_{2,(aq)} + 6\,NiOOH_{(s)} + H_2O_{(l)} \longrightarrow CO_{2,(g)} + N_{2,(g)} + 6\,Ni(OH)_{2,(s)} \quad (1)$$

$$Ni(OH)_{2,(s)} + OH^-_{(aq)} \rightleftharpoons NiOOH_{(s)} + H_2O_{(l)} + e^- \quad (2)$$

Reaction 3, hydrogen evolution, is used to balance the half reactions occurring on the anode. The overall electrolysis reaction is given by Reaction 4.

$$2\,H_2O_{(l)} + 2\,e^- \longrightarrow H_{2,(g)} + 2\,OH^- \quad (3)$$

$$CO(NH_2)_{2,(aq)} + H_2O_{(l)} \longrightarrow N_{2,(g)} + CO_{2,(g)} + 3\,H_{2,(g)} \quad (4)$$

The addition of nickel and other metals into nickel hydroxide has been shown to increase the electrode activity by altering the electronic structure and by expanding the electrochemically active surface area.[39–48] The inclusion of chromium oxide into nickel has been shown to depress the density of states at the Fermi level of the d-band of nickel, thereby weakening the Ni-O_{urea} bond and decreasing the energy for adsorption.[49] The inclusion of Mo into the nickel hydroxide films causes Ni to complete the $Ni(OH)_2$/NiOOH transition at lower onset potentials.[40] The onset potential for UOR is also lowered by the addition of Mo into Ni, as UOR is dependent on the presence of NiOOH. Doping of Mo promotes coupling of the N—N bond on the intramolecular level as well as the fracturing of the C=O in urea, promoting the selectivity of N_2 and CO_2 products.[50] Tafel slopes were lower on nickel iron hydroxide (57 mV dec^{-1}) than pure nickel (102 mV dec^{-1}), indicating that iron alters the potential dependence of UOR.[45] The inclusion of manganese into the oxide film allows for active nickel centers to reach a 3+ oxidation state at lower potentials, thus lowering the potential needed to drive UOR.[51]

An electrochemically-based WAK relies on two major components - the dialyzer and the dialysate regenerator. The dialysate regenerator is comprised of a urea removal cell, where the urea is electrochemically removed with a catalyst in an electrolyzer-type configuration. Previous studies have computationally modeled dialyzers for use in traditional dialysis and electrolyzers for use in commercial applications.[52–54] A model combining the two process elements has not been

previously seen before and is useful for determining operating parameters for a WAK. More importantly, the model is useful for finding pH of fluid downstream of the dialysate regenerator, as the production of CO_2 from Reac. 4 can affect the bicarbonate composition. Therefore, understanding urea electrooxidation on nickel-based catalysts is important for further development of the model, which is necessary to achieve a portable dialysis device.

This report combines incorporating electrochemical and model results for operation of an electrochemically-based WAK. Here, nickel-based electrocatalysts (Ni, NiMn, NiCr, NiMo, NiFe) were synthesized through a one-pot hydrothermal growth process. The electrochemical performance of each catalyst was investigated with cyclic voltammetry and staircase polarization techniques. Furthermore, the electrochemical performance of the catalysts was considered in a computationally-developed WAK model. The model was created to demonstrate the flowrates, urea concentrations, and pH of streams in contact with the dialyzer and the catalyst. Together, the catalysts and the model define and satisfy the criteria needed for development of a simplified dialysis device, setting the stage for future improvements.

2 Experimental

2.1 Electrochemical Cell

All electrochemical experiments were performed in a 150 mL three-electrode cell (Pine Research). Experiments were conducted in 0.5 M KOH with reagent grade concentrations of 0, 10, and 200 mM urea. The redox properties of nickel hydroxide have been seen to be affected by the presence of incidental iron (as low as 40 ppb) in the electrolyte. However, other groups have identified that nickel undergoes transformations with or without the presence of incidental iron in the electrolyte.[41,55,56] The concentration of iron was not monitored within this study, as there is assumed to be non-zero concentrations of iron in the dialysate in real-life applications.[57] A Pt coil ($\sim$ 5 cm^2) was used as the counter electrode, and a double-junction mercury oxide electrode (4.24 M KOH, $E^{\Theta}_{Hg/HgO}$ = 0.098 V, Pine Research) was used as the reference electrode. Since measurements were made in 0.5 M KOH, the reference electrode potential was adjusted for the liquid junction

potential (E_{LJP}) of –25.1 mV between 4.24 M KOH and 0.5 M KOH calculated with the stationary Nernst-Planck equation using LJPcalc software (https://swharden.com/LJPcalc).[58] Voltages are reported with respect to the reversible hydrogen electrode (RHE), calculated using the equation:

$$E_{RHE} = E_{Hg/HgO} + (0.059)\,pH + E^{\Theta}_{Hg/HgO} - E_{LJP} = E_{Hg/HgO} + 0.931 \quad (5)$$

The nickel transition and urea oxidation reaction onset potentials within this study are within 20 mV to those found in other reports, suggesting that the reference electrode and liquid junction potential are within an acceptable tolerance.[28,55]

The electrochemical experiments were controlled by a Solartron 1287 potentiostat. Cyclic voltammetry (CV) and staircase polarization experiments were performed at 37 °C with and without urea. Cyclic voltammetry was performed within a potential window that encompasses the $Ni(OH)_2$/NiOOH transition (Reaction 2) and oxygen evolution reactions. Cyclic potential sweeps from 0.90 to 1.60 V_{RHE} were conducted at 5 mV s^{-1}. The third CV scan was used for figures and analysis. Staircase potential step (polarization) experiments were conducted for steady-state analysis of UOR. For the staircase polarization experiments, the potential was stepped from 1.25 to 1.60 V_{RHE} in 10 mV increments at 20 min per step. Staircase polarization curves were generated by plotting the average of the last five minutes of current for a given step vs. the potential of that step.

2.2 Electrodes

Nickel foam (99.5 wt %, 95% porosity, Goodfellow) was laser cut to 1 cm^2 pieces and used as a substrate for hydrothermal growth. The nickel foam (NiF) was sequentially sonicated in deionized water (DI, Millipore-Q water system), ethanol (95 wt.%, Fisher-Scientific), and 3 M HCl (Macron Fine Chemicals) for 10 minutes each to remove any contaminants before being placed in the hydrothermal growth chamber. The percentage of metal grown on the working electrode was targeted to be 1 mol%, with the remaining as nickel. Metallic salts of 1.00 mg of $Cr(NO_3)_3 \cdot 9H_2O$ (99.9 wt.%, Acros Organics), 1.01 mg of $Fe(NO_3)_3 \cdot 9H_2O$ (99.95 wt.%, Aldrich), 0.39 mg of $KMnO_4$

(>99 wt.%, Fisher-Scientific), and 1.75 mg of $(NH_4)_6Mo_7O_{24} \cdot 4H_2O$ (99.97 wt.%, Aldrich) were added and mixed with 20 mL DI water in separate vials. Then, 72 mg $Ni(NO_3)_2 \cdot 6H_2O$ (99.9 wt.%, Acros Organics) and 150 mg urea (99.6 wt. %, Fisher-Scientific) were added and mixed into each vial. The solutions were individually transferred into a 25 mL Teflon-lined stainless-steel hydrothermal vessel. Four pieces of NiF were placed vertically into the solution in the vessel. The vessel was sealed and placed in a 105 °C oven for 12 hours. The vessel was cooled to room temperature before opening. The hydrothermally grown NiF pieces were sonicated sequentially in DI water and ethanol for 10 minutes each to remove loose particulates. Each electrode was imaged with a scanning electron microscope (SEM, ThermoFisher Scientific Apreo-Symmetry with Ultimax 100) equipped with an energy dispersive spectrometer (EDS). The mol % loading for each electrode was confirmed with elemental analysis by EDS.

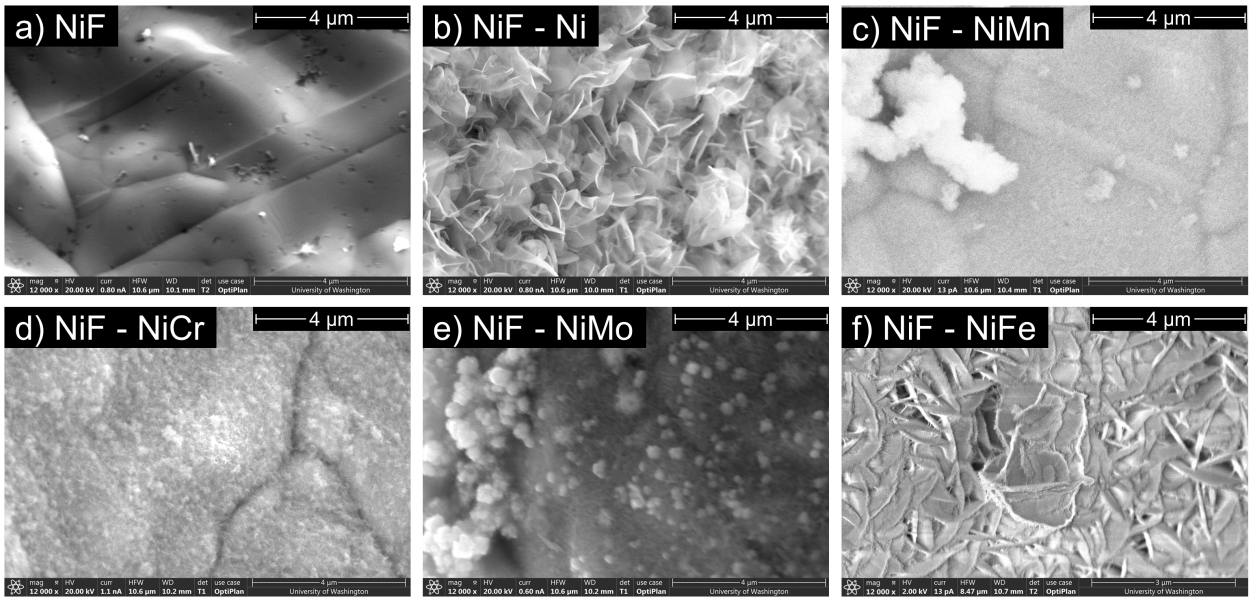

Figure 2: Scanning electron microscopy images taken at 12,000x magnification of a) nickel foam (NiF) and metallic species b) Ni, c) NiMn, d) NiCr, e) NiMo, and f) NiFe grown on NiF prior to experimentation.

Ni(M)	Ni	M
Ni	100.00	0.00
NiMn	99.30	0.70
NiCr	99.30	0.70
NiMo	99.18	0.82
NiFe	99.56	0.44

Table 1: Mole % composition of metal species (M) grown on nickel foam, ignoring oxygen content.

3 Results

3.1 SEM/EDS

Scanning electron microscopy images taken at 12,000x magnification for nickel-based electrodes used in this study are seen in Fig. 2. The NiF electrode showed a smooth surface, while grown species exhibit a change in surface morphology. NiF-Ni and NiF-NiFe growths form platelets that are similar to surfaces seen in literature (Fig. 2b, f).[28,59] NiF-NiMn and NiF-NiMo growths form large crystalline nodes (Fig. 2c, e). NiF-NiCr does not form large crystalline structures, but rather evenly coats the surface with a rough mossy texture (Fig. 2d). The compositions of the grown metallic species was confirmed by EDS and are seen in Table 1 and in elemental maps in the Supplementary Information.

3.2 Nickel Transition And Oxygen Evolution

Cyclic voltammetry scans of 0, 10, and 200 mM urea in 0.5 M KOH for nickel foams are presented in Figure 3. Currents for the grown species exceed those for NiF for all cases. The urea-free nickel transition onset potential can be seen for all electrodes near 1.36 V_{RHE} on the forward scan, except for NiF-NiMn, which has the lowest onset of $\sim$1.33 V_{RHE}. The NiF electrode exhibits a narrow peak at 1.36 V (inset of Fig. 3 a) while the grown species show a single, wide peak. At higher potentials, the current increases sharply due to the onset of oxygen evolution reaction (OER, $\sim$1.50 V_{RHE}). The grown species show an increase in OER current compared to NiF, with NiF-NiFe showing the largest OER current at 1.60 V_{RHE}.

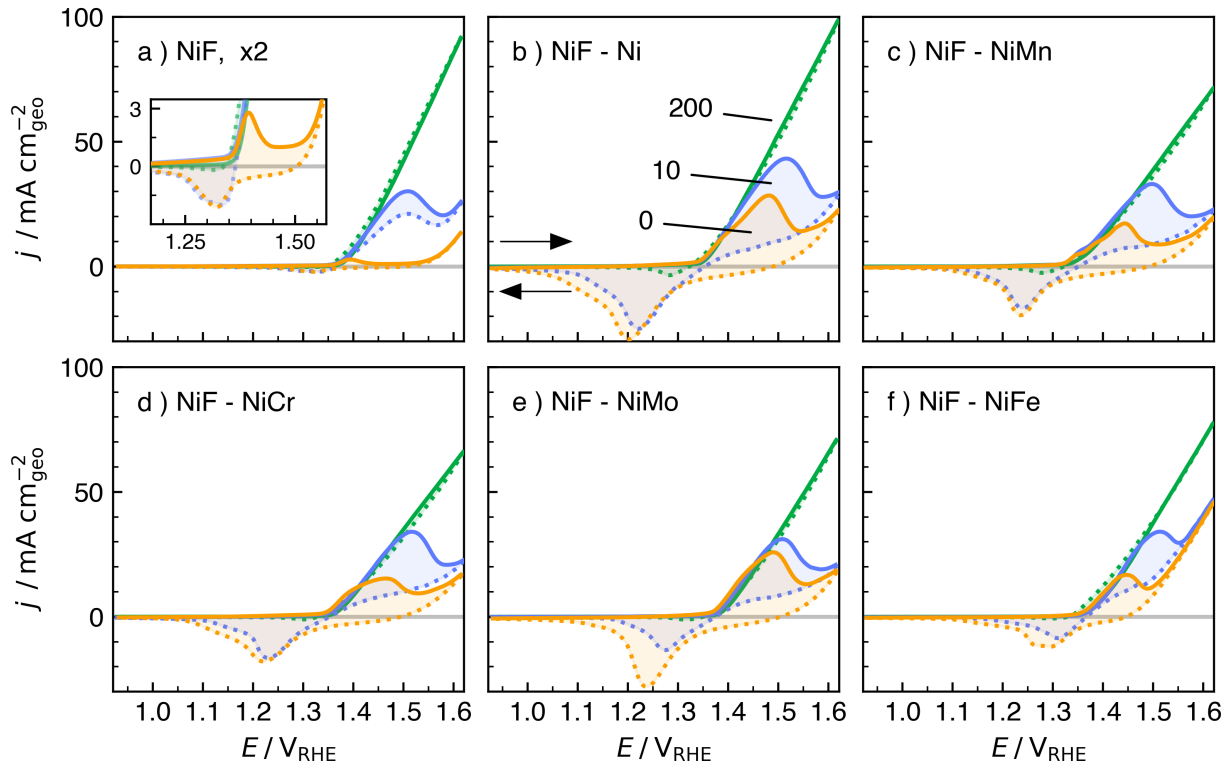

Figure 3: Cyclic voltammetry scans (5 mV s^{-1}) of a) nickel foam (NiF) and metallic species b) Ni, c) NiMn, d) NiCr, e) NiMo, and f) NiFe grown on NiF for concentrations of 0 (orange), 10 (blue), and 200 (green) mM urea in 0.5 M KOH at 37 °C. The solid line on the CV indicates the forward scan while the dotted line indicates the reverse scan. The current for NiF is scaled by 2 to include the curves on the same y-axis.

The reverse sweep shows the reduction of NiOOH back to $Ni(OH)_2$. All grown species show a single reduction peak, but NiF-NiFe exhibits a flattened peak from 1.31–1.27 V_{RHE} suggesting a second peak.

Staircase polarization curves (SPC) for 0, 10, and 200 mM urea for all electrodes are presented in Figure 4. The 0 mm plots for all electrodes show no current during potentials where $Ni(OH)_2$/NiOOH occurs, indicating that steady state was achieved. The current increases near 1.48 V_{RHE} as the potential is large enough to begin OER. At 1.63 V_{RHE}, the rightmost point in the plots, all electrodes exhibit similar currents near 33 mA cm^{-2}_{geo}, except NiF and NiF-NiFe. NiF-NiFe has the largest OER current compared to the other electrodes, in agreement with other studies of iron-containing electrodes that show improved oxygen evolution kinetics.[28,55,56,60,61]

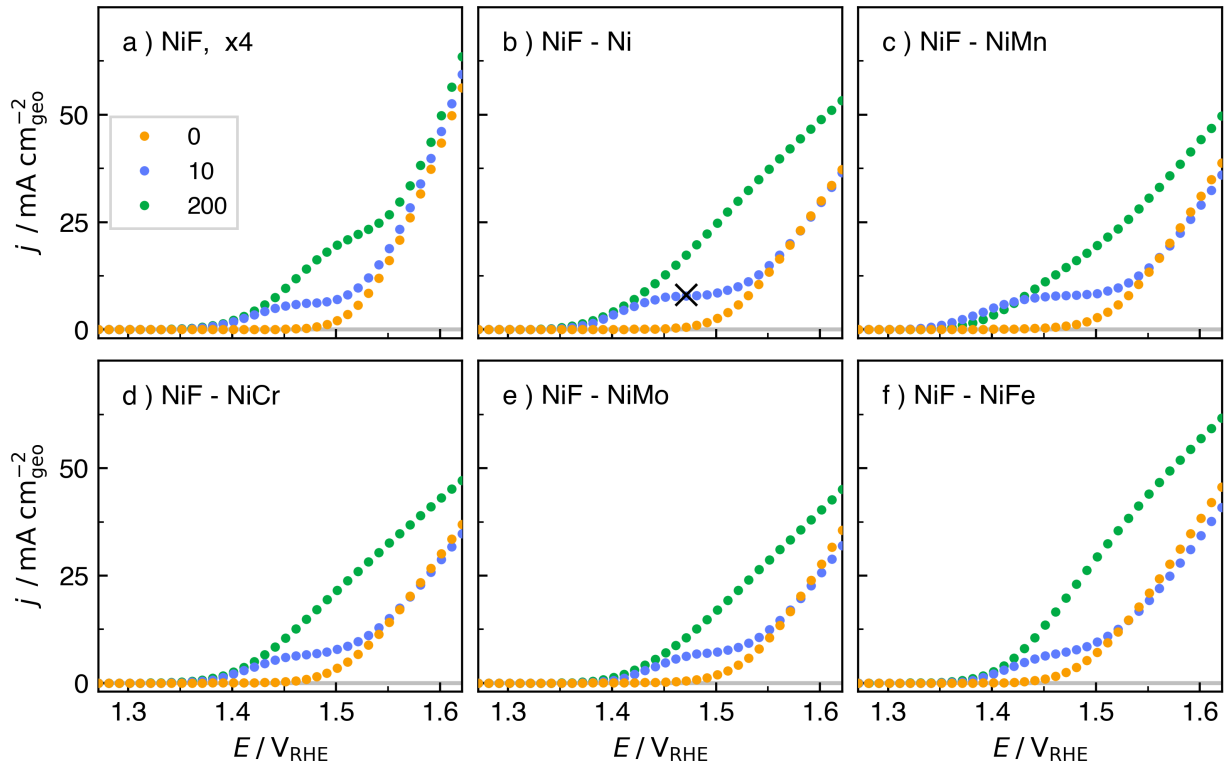

Figure 4: Staircase polarization curves of a) nickel foam (NiF) and metallic species b) Ni, c) NiMn, d) NiCr, e) NiMo, and f) NiFe grown on NiF for concentrations of 0, 10, and 200 mM urea in 0.5 M KOH. The catalyst and potential shown in Figure 9 is designated by an 'X' for NiF-Ni at 1.45 V_{RHE}, respectfully. The current for NiF is scaled by 4 to include the points on the same y-axis.

3.3 Urea oxidation

Urea electrooxidation was performed at 10 mM urea to understand performance under dialysate-relevant solutions and in 200 mM urea to probe UOR kinetics. The 10 and 200 mM CV responses are seen in Fig. 3. For both 10 and 200 mM, the current is essentially zero from 0 up to 1.36 V_{RHE} since UOR does not occur on $Ni(OH)_2$. Urea oxidation begins near the same potential as the $Ni(OH)_2$/NiOOH onset potential, as there is now NiOOH on the surface. The 10 mM current continues to increase until a mass transfer limitation is reached, as seen by a peak in Fig. 3. The mass transfer limit is semi-consistent amongst the grown species. The 200 mM CV response is not impeded by a mass transfer limitation, however OER may be participating on the surface at potentials greater than 1.53 V_{RHE}.

The reverse scans exhibit similar behaviors for all electrodes in Fig. 3. The reduction peak is smaller with the addition of urea because urea consumes nickel sites by a catalyst regeneration mechanism, converting NiOOH back to $Ni(OH)_2$ as seen in Reac. 2. Higher concentrations of urea cause the reduction peak to be small, as seen by comparison of 10 and 200 mM curves in Fig. 3.

Staircase polarization curves for 10 and 200 mM urea for all electrodes are seen in Figure 4. The 10 mM curves start to plateau at 1.46 V_{RHE} for all cases due to the mass transfer limitation. The mass transfer limitation occurs at nearly the same current ($\sim$ 9 mA cm^{-2}_{geo}) for all grown species. For all cases, 0 and 10 mM currents at 1.60 V_{RHE} were similar, suggesting OER was the dominant reaction on the surface. The 200 mM responses, except NiF, all show an increase in current at OER-relevant potentials (> 1.48 V_{RHE}) beyond the 10 mM responses in the SPC. The currents for 0, 10, and 200 mM on NiF indicate that OER is dominant from 1.58–1.63 V_{RHE}.

3.4 Model

A simplified dialysis model was created and evaluated to gauge the viability of the synthesized catalysts for a WAK. The two main components, the dialyzer and the regenerator, were modeled with specifications applicable to a WAK:

- Remove 30 g urea of during an 8 hour operation (3.75 g urea hr^{-1});
- Accommodate flow rates up to 300 mL min^{-1} from the dialyzer[62] and;
- Conduct hemodialysis without a continuous water source.

A diagram of the continuous dialysis unit is seen in Figure 5. Blood flows from the patient into the dialyzer, where urea crosses over from the blood loop into the dialysate loop due to a concentration gradient. The dialysate flows into the urea removal cell (URC) where urea is removed *via* Reac. 1. The dialysate leaves the URC and enters the dialyzer to receive more urea from blood.

The dialyzer is based on a hollow-fiber and tube mass exchanger. Blood flows through hollow fibers, where small solutes and ions can migrate to the dialysate by diffusion and convection.[63] Sherwood numbers of hollow-fiber dialyzers tend to be large to induce higher fluxes of uremic toxins and middle-molecular weight solutes.[64–66] Toxins other than urea are not included in the

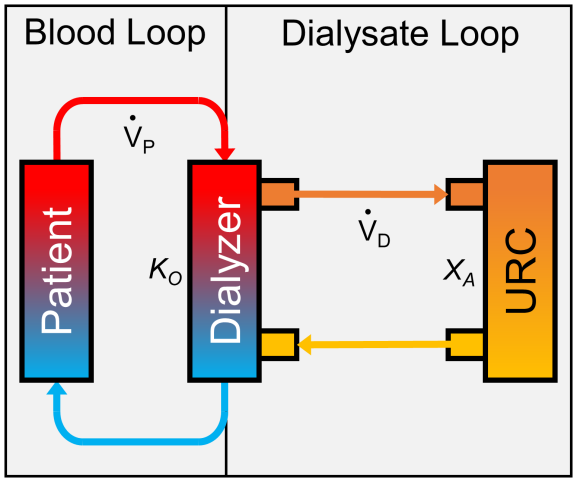

Figure 5: Simplified model of a portable dialysis unit. Blood flows from the patient through a dialyzer, where the urea transfers to the dialysate for removal by the urea removal cell (URC).

systems of equations, but can be added in the future. The dialyzer is designed for counter-current operation to maximize urea removal. The dialyzer was modeled with the mass transfer and mass balance, Eqs. 6 and 7, respectively:

$$N_u = K_O A \, \Delta C_{u,lm} \tag{6}$$

$$\dot{V}_{P,i} C_{u,P,i} - \dot{V}_{P,o} C_{u,P,o} \;=\; \dot{V}_{D,i} C_{u,D,i} - \dot{V}_{D,o} C_{u,D,o} \tag{7}$$

where N_u is the flux of urea through the dialyzer membrane, $K_O A$ is the mass transfer coefficient with area (units of mL min^{-1}), P is the patient side, D is the dialysate side, and $\dot{V}$ and C_u are volumetric flowrate and urea concentration, respectively, of inlets i and outlets o.

The anolyte chamber of the URC was modeled as a continuous stirred tank reactor. The URC extent of reaction was set as a design variable for calculation simplicity.[67–69] The extent of reaction was based on the urea electrooxidation half reaction in Reac. 1. The model uses the following equations to find the changes in molar flows through the URC:

$$\dot{n}_{N_2} = \dot{n}_{CO_2} = \dot{V}_{D,i} C_u X_A \tag{8}$$

$$\dot{n}_{H_2O,m} = 6\,\eta \dot{V}_{D,i} C_u X_A \tag{9}$$

$$\dot{n}_{H_2O,g} = \frac{2\,\dot{V}_{D,i} C_u X_A P_s}{P} \tag{10}$$

$$\dot{n}_{H_2O,l} = \dot{V}_{D,i} - \dot{n}_{H_2O,g} + \dot{n}_{H_2O,m} + 5\,\dot{V}_{D,i} C_u X_A \tag{11}$$

$$\dot{n}_u = \dot{V}_{D,i} C_u (1 - X_A) \tag{12}$$

where $\dot{n}$ is the molar flow rate per respective species, $\dot{V}_{D,i}$ volumetric flowrate of fluid into the URC, C_u is the concentration of urea, X_A is extent of reaction, η is the osmotic drag coefficient through the membrane (m), P is the total pressure (760 torr), and P_s is the saturation pressure of water at 37°C. Water molecules are able to cross over from the cathode compartment to the anode compartment due to osmotic drag, which is proportionally related to the number of hydroxide ions generated from Reac. 1 and the osmotic drag coefficient.[70] The osmotic drag coefficient is constant for this study, but depends on reaction conditions and can be tuned accordingly for increased model accuracy.

3.5 Model Trends

A system of the combined dialyzer and URC was modeled over a range of flow and urea concentration conditions. An array of K_OA (200 - 400 mL min^{-1}) and X_A (0.4 - 1) values was used to calculate flowrates, concentrations in and out of the dialyzer, and pH of dialysate after the URC, as seen in Figure 6. The model, for example, provided urea concentrations of 1.6 and 8.2 mM of dialysate entering and exiting the dialyzer at 160 mL min^{-1}, respectively, while showing that the pH drops from 7.4 to 7.1 for an X_A of 0.8 and a K_OA of 231 mL min^{-1} (Fig. 6, F3).

At a low extent of reaction, the URC is not able to remove enough urea to substantially lower

the concentration entering the dialyzer, as seen by Fig. 6a. A low extent of reaction also requires a high mass flowrate of urea to enter the URC, thus requiring a high volumetric flowrate of dialysate through the dialyzer in order to remove 3.75 g urea hr^{-1}. A high extent of reaction lowers the urea concentration entering the dialyzer (with 0 mM at 100 % X_A), maximizing the flux of urea from blood across the dialyzer. A high extent of reaction consumes urea faster, thereby allowing for a low flowrate to be achieved. A larger extent of reaction also produces more CO_2, which reduces the solution pH, as seen in Fig. 6d. As CO_2 is produced on the anode, a fraction of CO_2 reacts with H_2O to form H_2CO_3, a weak acid that dissociates to form H^+ and HCO_3^-.[71]

Fresnius F3 and F4 dialyzers are included in Fig. 6 to show the performance of commonly used, commercially available products.[72–74] Larger mass transfer coefficients allow for more urea to move through the dialyzer membrane, as seen by the increase in concentration along the arrow in Fig. 6b. The Fresnius F4 has a higher K_OA value than the F3 (374 > 231 mL min^{-1}), allowing for the system to operate with a lower extent of reaction.

4 Discussion

4.1 Electrochemical surface area

The electrochemical surface area (A_{ECSA}) of each electrocatalyst was determined by finding the number of sites participating in the $Ni(OH)_2$/NiOOH transition. The number of sites was calculated by integrating the reverse sweep where current was less than 0 mA. The A_{ECSA} was calculated by correlating the number of sites to the average cell density of the NiOOH plane by Equation 13

$$A_{ECSA} = \frac{Q_r N_A}{nF\Gamma} \tag{13}$$

where Q_r is the NiOOH reduction charge, N_A is Avogadro's number, n is the number of electrons involved in $Ni(OH)_2$/NiOOH (1 e^-, Reac. 2), F is Faraday's constant, and Γ is the NiOOH site density. An average Γ value of 5.7×10^{14} cm^{-2} was calculated based on a lattice parameter of 0.283 nm.[75] Q_{red} was calculated by integrating the CV in Fig. 3 between the potential where

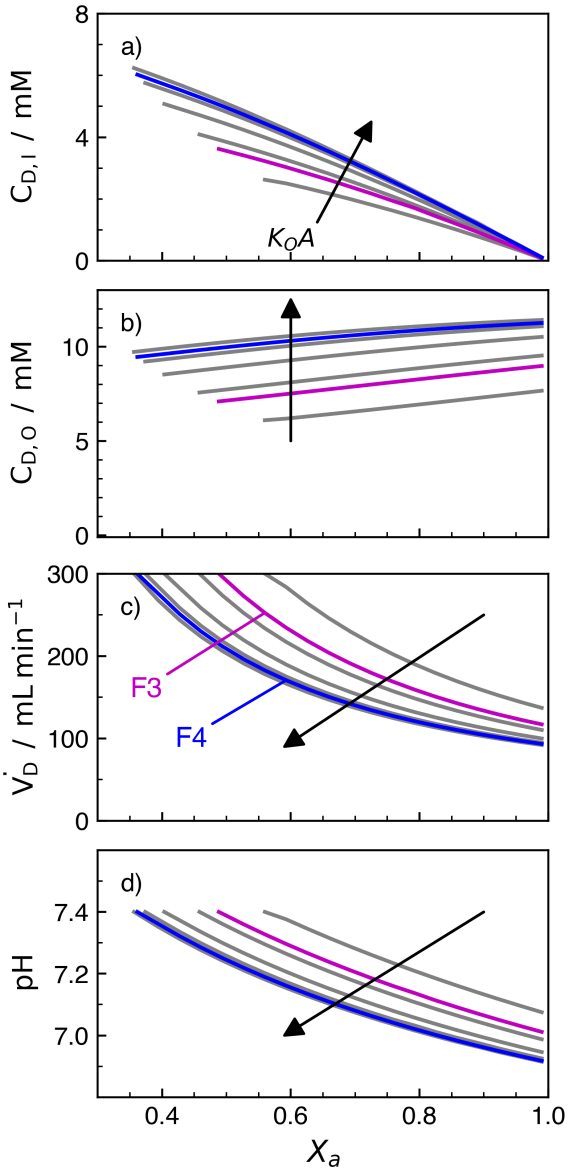

Figure 6: Model output for: concentration of urea flowing a) in and b) out of the dialyzer, c) flowrate into the dialyzer, and d) pH of fluid flowing into the dialyzer. Arrows indicate an increase in mass transfer coefficient (K_OA). Fresnius F3 and F4 are commercially available dialyzers with mass transfer coefficients of 231 and 374 mL min^{-1}, respectively.[72–74]

current becomes reducing ($\sim$ 1.48 V_{RHE}) and 0.90 V_{RHE}.

Values for A_{ECSA} are presented in Figure 7. The grown species increased the physical surface area within the pores of NiF (seen in Fig. 2), thereby increasing ECSA and allowing more active sites to participate in $Ni(OH)_2$/NiOOH reaction. The ECSA of grown species was within an order of magnitude with each other. NiF-NiFe had a smaller ECSA than NiF-Ni, but had similar platelet

structures (Fig. 2a,f). NiF-NiFe and NiF-NiCr had the similar ECSAs, despite different crystal morphologies.

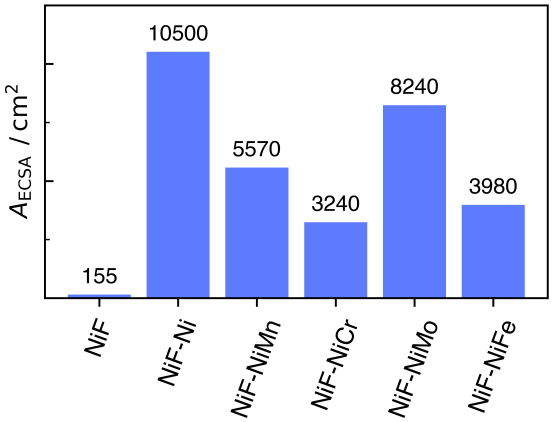

Figure 7: Electrochemical surface area (A_{ECSA}) for nickel foam (NiF) and metallic species. The metallic species were grown on a NiF precursor *via* a hydrothermal method.

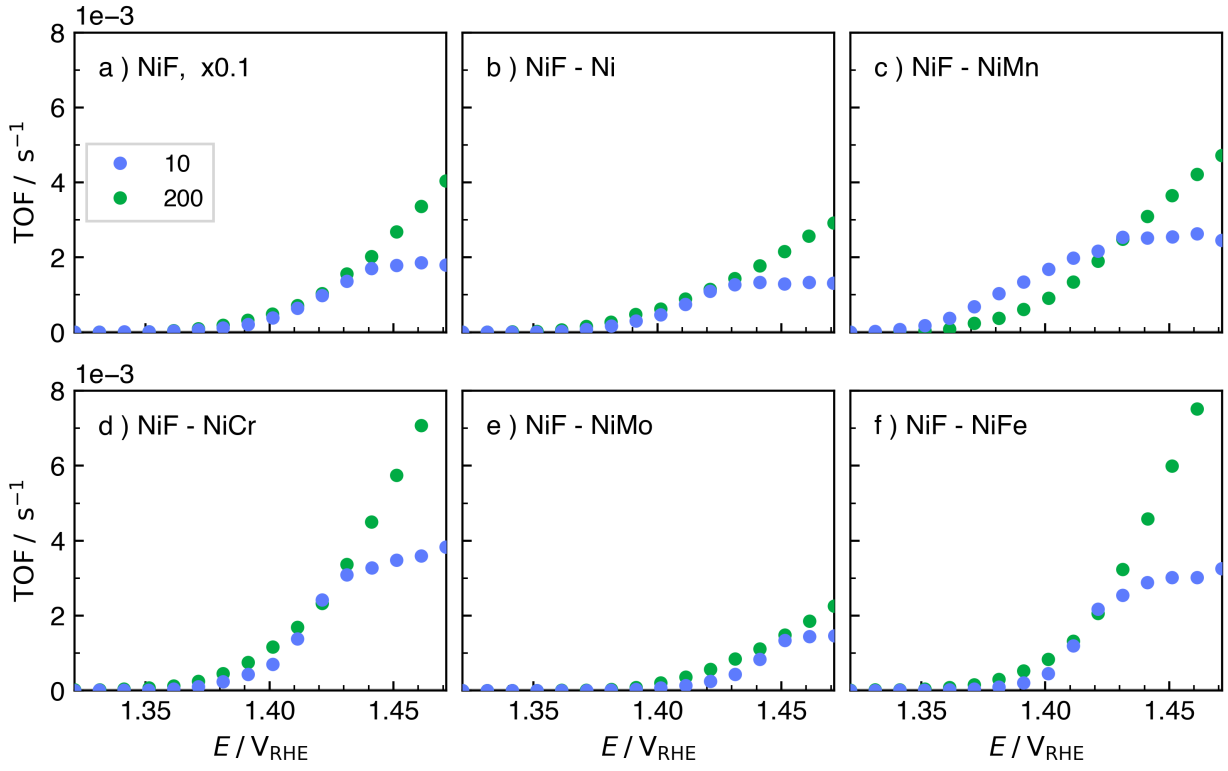

Figure 8: Turnover Frequency (TOF) of a) nickel foam (NiF) and metallic species b) Ni, c) NiMn, d) NiCr, e) NiMo, and f) NiFe grown on NiF for concentrations of 0, 10, and 200 mM urea in 0.5 M KOH. The TOF for NiF is scaled by 0.2 to include the points on the same y-axis.

4.2 *Turnover Frequency*

The 10 and 200 mM urea staircase polarization curves were used to determine turnover frequencies (TOF) on a per-site kinetic analysis. The TOF was examined over a potential range of 1.30–1.45 V_{RHE} to avoid current associated with OER. The TOF is given by

$$\text{TOF} = \frac{i_{SPC} N_A}{F n N_S} = \frac{i_{SPC} N_A}{F\ n_u\ \Gamma\ A_{ECSA}} \tag{14}$$

where i_{SPC} is the staircase polarization current, n_u is number of electrons involved in UOR (6 e^-, Reac. 1), and N_S is the number of NiOOH sites. The 10 and 200 mM TOFs for all electrodes are seen in Figure 8. Although the SPC data continues past 1.45 V_{RHE}, oxygen evolution becomes large and skews the conclusions drawn for UOR kinetics. The TOFs level off after $\sim$ 1.41 V_{RHE} as a mass transfer limitation is reached for 10mM urea, but otherwise follow the same trend as the 200 mM TOF.

NiF-based grown species had UOR TOF values similar to electrodes seen in literature.[76–78] The hydrothermal growth increased the number of active sites from NiF, as seen by the A_{ECSA} in Fig. 7, but decreased the UOR kinetics of NiF based on the TOF analysis. Growing more sites allowed for more urea to oxidize, but at a slower rate per site.

4.3 *Implementation*

The synthesized electrodes provided values that, when combined with the results of the model, show operation parameters necessary for a simplified dialysis device. All electrodes with grown species electrodes exhibited similar currents towards UOR due to the mass transfer limitation between 1.40 and 1.45 V_{RHE}. The NiF-Ni catalyst was chosen to be paired with the model due to its single element composition.

Figure 9 shows the performance of a NiF-Ni electrode (operating at 7.64 mA cm^{-2} at 1.45 V_{RHE}, as seen in Fig. 4) with four different sizes of geometric area for a dialyzer flowrate of 200 mL min^{-1}. The curve represents the performance of a Fresnius F4 dialyzer (K_OA of 374 mL

min^{-1}), where the shaded area shows the flowrates and extent of reaction of catalysts that remove $\geq$ 3.75 g urea hr^{-1}. Fig. 9I represents a current of 7.64 mA cm^{-2}, which is beneath the curve and is not usable in the WAK for any dialyzer flowrate. However, the geometric area of the catalyst can be expanded to increase the current supplied to the anode, increasing the rate of urea removal. Fig. 9III represents the lowest geometric area needed (1314 cm^2) to remove 3.75 g urea hr^{-1} at a 200 mL min^{-1} dialyzer flowrate. Fig. 9IV represents an area of 2000 cm^2, which obtains an extent of reaction higher than necessary for operation. However, large, planar areas necessary for a URC may impinge on the portability of the system.

A rough estimate of URC size can be made on the basis of a total area of 2,000 cm^2, which allows for de-rated electrooxidation performance. For a single cell of 100 cm^2 and spacing between cells of 0.5 cm, the size of the electrolysis stack would be 10 x 10 x 10 cm^3 (1 liter). This estimate includes only the electrodes and flow field plates. A conservative estimate of ancillary hardware (compression plates, manifolds, tabulation, etc.) is a volume equal to that of the URC. This brings the total reactor volume to approximately 2 liters. This is a large volume for a portable dialysis device and clearly needs to be reduced. Because of the mass transfer limit of dilute urea solutions, further URC development should be focused on improving mass transfer.

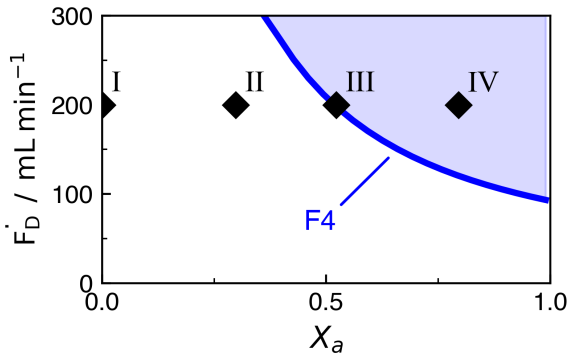

Figure 9: Performance of NiF-Ni catalyst with 1 (I), 750 (II), 1314 (III), and 2000 (IV) cm^2 with a dialyzer flowrate of 200 mL min^{-1}. The line represents the model output for a Fresnius F4 dialyzer (K_OA: 374 mL min^{-1}).[72] Points in the shaded region are acceptable for use in the simplified dialysis device.

5 Conclusion

Nickel-based catalysts were developed by a hydrothermal growth procedure to include Ni, NiMn, NiCr, NiMo, and NiFe deposited on nickel foam to improve the urea oxidation current density for application in a wearable artificial kidney. The grown species increase the electrochemically active surface area and roughness of the electrode. Although the electrochemically active surface area is increased, a mass transfer limitation is reached with 10 mM urea for all grown metallic electrodes. Urea oxidation kinetics were investigated using non-dialysate concentrations of urea (200 mM), as reaction was not limited by mass transfer. The grown electrodes had the highest currents during staircase polarization, but NiF exhibited TOFs an order of magnitude or more greater than that of the grown electrodes.

A simplified dialysis model was created to evaluate the viability of nickel-based catalysts by establishing necessary flowrates, urea concentrations, and pH of streams as a function of the dialyzer mass transfer coefficient and the URC extent of reaction. The performance of a NiF-Ni electrode was evaluated in the computational model of a continuous dialysis system. The minimum required area is 1,314 cm^2 to remove 3.75 g urea hr^{-1} for a Fresnius F4 dialyzer flowrate of 200 mL min^{-1}. Together, the model and the catalysts provided operating conditions of a simplified, continuous dialysis system, setting the stage for future improvements.

6 Acknowledgements

Part of this work was conducted at the Molecular Analysis Facility, a National Nanotechnology Coordinated Infrastructure (NNCI) site at the University of Washington, which is supported in part by funds from the National Science Foundation (awards NNCI-2025489, NNCI-1542101), the Molecular Engineering & Sciences Institute, and the Clean Energy Institute. The authors thank the members of Center for Dialysis Innovation for the shared knowledge of dialysis systems. The authors also thank Prof. Peter Strasser and Prof. Gregory Jerkiewicz for the shared knowledge of nickel hydroxide catalysts in electrochemical systems.

7 Funding Sources

Major funding was provided by the National Science Foundation [grant NSF/CBET: 2055257]. Initial support was provided by the Northwest Kidney Centers and the Center for Dialysis Innovation at the University of Washington

Plain Language Summary

Nickel particles were incorporated on nickel foams to enhance the removal of urea for concentrations relevant to dialysis for the development of a wearable artificial kidney. The performance of the synthesized catalysts was assessed when integrated into a simplified dialysis model.

Graphical Abstract

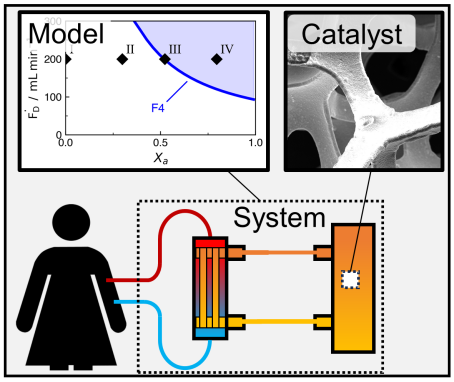

References

1. Burrows, N. R., Koyama, A. & Pavkov, M. E. Reported Cases of End-Stage Kidney Disease — United States, 2000–2019. *MMWR. Morbidity and Mortality Weekly Report* **71,** 412–415. doi:10.15585/mmwr.mm7111a3 (Mar. 2022).

2. Gura, V., Rivara, M. B., Bieber, S., Munshi, R., Smith, N. C., Linke, L., Kundzins, J., Beizai, M., Ezon, C., Kessler, L. & Himmelfarb, J. A wearable artificial kidney for patients with end-stage renal disease. *JCI Insight* **1.** doi:10.1172/jci.insight.86397 (June 2016).

3. Mapes, D. L., Lopes, A. A., Satayathum, S., Mccullough, K. P., Goodkin, D. A., Locatelli, F., Fukuhara, S., Young, E. W., Kurokawa, K., Saito, A., Bommer, J., Wolfe, R. A., Held, P. J. & Port, F. K. Health-related quality of life as a predictor of mortality and hospitalization: The Dialysis Outcomes and Practice Patterns Study (DOPPS). *Kidney International* **64,** 339–349. doi:10.1046/j.1523-1755.2003.00072.x (July 2003).

4. Evans, R. W., Manninen, D. L., Garrison, L. P., Hart, L. G., Blagg, C. R., Gutman, R. A., Hull, A. R. & Lowrie, E. G. The Quality of Life of Patients with End-Stage Renal Disease. *New England Journal of Medicine* **312,** 553–559. doi:10.1056/NEJM198502283120905 (Feb. 1985).

5. Chiu, Y.-W., Teitelbaum, I., Misra, M., de Leon, E. M., Adzize, T. & Mehrotra, R. Pill Burden, Adherence, Hyperphosphatemia, and Quality of Life in Maintenance Dialysis Patients. *Clinical Journal of the American Society of Nephrology* **4,** 1089–1096. doi:10.2215/CJN.00290109 (June 2009).

6. Carpenter, K. & Stuve, E. M. Electrooxidation of urea and creatinine on nickel foam-based electrocatalysts. *Journal of Applied Electrochemistry* **51,** 945–957. doi:10.1007/s10800-021-01545-1 (June 2021).

7. Locatelli, F., La Milia, V., Violo, L., Del Vecchio, L. & Di Filippo, S. Optimizing haemodialysate composition. *Clinical Kidney Journal* **8,** 580–589. doi:10.1093/ckj/sfv057 (Oct. 2015).

8. Desai, N. Basics of base in hemodialysis solution: Dialysate buffer production, delivery and decontamination. *Indian Journal of Nephrology* **25,** 189. doi:10.4103/0971-4065.147369 (2015).

9. Magnani, S. & Atti, M. Uremic Toxins and Blood Purification: A Review of Current Evidence and Future Perspectives. *Toxins* **13,** 246. doi:10.3390/toxins13040246 (Mar. 2021).

10. Van Gelder, M. K., Jong, J. A., Folkertsma, L., Guo, Y., Blüchel, C., Verhaar, M. C., Odijk, M., Van Nostrum, C. F., Hennink, W. E. & Gerritsen, K. G. Urea removal strategies for dialysate regeneration in a wearable artificial kidney. *Biomaterials* **234,** 119735. doi:10.1016/j.biomaterials.2019.119735 (Mar. 2020).

11. Wernert, V., Schäf, O., Ghobarkar, H. & Denoyel, R. Adsorption properties of zeolites for artificial kidney applications. *Microporous and Mesoporous Materials* **83,** 101–113. doi:10.1016/j.micromeso.2005.03.018 (Sept. 2005).

12. Giordano, C., Esposito, R., Bello, P., Quarto, E. & Gonzalez, F. M. Cold Carbon Apparatus for Hemodialysis. *Journal of Dialysis* **1,** 165–179. doi:10.3109/08860227609039143 (Jan. 1976).

13. Hu, G., Pojman, J. A., Scott, S. K., Wrobel, M. M. & Taylor, A. F. Base-Catalyzed Feedback in the Urea-Urease Reaction. *The Journal of Physical Chemistry B* **114,** 14059–14063. doi:10.1021/jp106532d (Nov. 2010).

14. Grinval'd, V. M., Leshchinskii, G. M., Rodin, V. V., Strelkov, S. I. & Yakovleva, A. A. Development and Testing of a Unit for Electrochemical Oxidation of Products of Hemodialysis. *Biomedical Engineering* **37,** 67–72. doi:10.1023/A:1024727513884 (2003).

15. Köster, K., Wendt, H., Gallus, J., Krisam, G. & Lehmann, H. D. Regeneration of Hemofiltrate by Anodic Oxidation of Urea. *Artificial Organs* **7,** 163–168. doi:10.1111/j.1525-1594.1983.tb04182.x (May 1983).

16. Keller, R. W., Yao, S. J., Brown, J. M., Wolfson, S. K. & Zeller, M. V. Electrochemical removal of urea from physiological buffer as the basis for a regenerative dialysis system. *Journal of Electroanalytical Chemistry and Interfacial Electrochemistry* **116,** 469–485. doi:10.1016/S0022-0728(80)80271-3 (Jan. 1980).

17. Hintzen, K., Stiller, S., Brunner, H., Rautenbach, R. & Mann, H. Electrodialysis and Reverse Osmosis as a Regeneration System for Hemofiltrate. *Artificial Organs* **7,** 169–175. doi:10.1111/j.1525-1594.1983.tb04183.x (May 1983).

18. Fels, M. Recycle of dialysate from the artificial kidney by electrochemical degradatian of waste metabolites: Small-scale laboratory investigations. *Medical & Biological Engineering & Computing* **16,** 25–30. doi:10.1007/BF02442928 (Jan. 1978).

19. Fels, M. Recycle of dialysate from the artificial kidney by electrochemical degradation of waste metabolites: Continuous reactor investigations. *Medical & Biological Engineering & Computing* **20,** 257–263. doi:10.1007/BF02442789 (May 1982).

20. Wester, M., Simonis, F., Lachkar, N., Wodzig, W. K., Meuwissen, F. J., Kooman, J. P., Boer, W. H., Joles, J. A. & Gerritsen, K. G. Removal of Urea in a Wearable Dialysis Device: A Reappraisal of Electro-Oxidation. *Artificial Organs* **38,** 998–1006. doi:10.1111/aor.12309 (Dec. 2014).

21. Wester, M., van Gelder, M. K., Joles, J. A., Simonis, F., Hazenbrink, D. H. M., van Berkel, T. W. M., Vaessen, K. R. D., Boer, W. H., Verhaar, M. C. & Gerritsen, K. G. F. Removal of urea by electro-oxidation in a miniature dialysis device: a study in awake goats. *American Journal of Physiology-Renal Physiology* **315,** F1385–F1397. doi:10.1152/ajprenal.00094.2018 (Nov. 2018).

22. Groth, T., Stegmayr, B. G., Ash, S. R., Kuchinka, J., Wieringa, F. P., Fissell, W. H. & Roy, S. Wearable and implantable artificial kidney devices for end-stage kidney disease treatment: Current status and review. *Artificial Organs* **47,** 649–666. doi:10.1111/aor.14396 (Apr. 2023).

23. Tatarchuk, S. W., Medvedev, J. J., Li, F., Tobolovskaya, Y. & Klinkova, A. Nickel-Catalyzed Urea Electrolysis: From Nitrite and Cyanate as Major Products to Nitrogen Evolution. *Angewandte Chemie International Edition* **61.** doi:10.1002/anie.202209839 (Sept. 2022).

24. Neth, M. R., Love, J. S., Horowitz, B. Z., Shertz, M. D., Sahni, R. & Daya, M. R. Fatal Sodium Nitrite Poisoning: Key Considerations for Prehospital Providers. *Prehospital Emergency Care* **25,** 844–850. doi:10.1080/10903127.2020.1838009 (Nov. 2021).

25. Hoenich, N. A. & Ronco, C. Haemodialysis Fluid: Composition and Clinical Importance. *Blood Purification* **25,** 62–68. doi:10.1159/000096400 (2007).

26. Huang, L.-F., Hutchison, M. J., Santucci, R. J., Scully, J. R. & Rondinelli, J. M. Improved Electrochemical Phase Diagrams from Theory and Experiment: The Ni–Water System and Its Complex Compounds. *The Journal of Physical Chemistry C* **121,** 9782–9789. doi:10.1021/acs.jpcc.7b02771 (May 2017).

27. Yan, W., Wang, D. & Botte, G. G. Electrochemical decomposition of urea with Ni-based catalysts. *Applied Catalysis B: Environmental* **127,** 221–226. doi:10.1016/j.apcatb.2012.08.022 (Oct. 2012).

28. Xie, J., Liu, W., Lei, F., Zhang, X., Qu, H., Gao, L., Hao, P., Tang, B. & Xie, Y. Iron-Incorporated α-Ni$(OH)_2$ Hierarchical Nanosheet Arrays for Electrocatalytic Urea Oxidation. *Chemistry - A European Journal* **24,** 18408–18412. doi:10.1002/chem.201803718 (Dec. 2018).

29. Xu, W., Wu, Z. & Tao, S. Urea-Based Fuel Cells and Electrocatalysts for Urea Oxidation. *Energy Technology* **4,** 1329–1337. doi:10.1002/ente.201600185 (Nov. 2016).

30. Klapper, H. S., Zadorozne, N. S. & Rebak, R. B. Localized Corrosion Characteristics of Nickel Alloys: A Review. *Acta Metallurgica Sinica (English Letters)* **30,** 296–305. doi:10.1007/s40195-017-0553-z (Apr. 2017).

31. Al-Malahy, K. S. & Hodgkiess, T. Comparative studies of the seawater corrosion behaviour of a range of materials. *Desalination* **158,** 35–42. doi:10.1016/S0011-9164(03)00430-2 (Aug. 2003).

32. Henderson, J., Ebrahimi, N., Dehnavi, V., Guo, M., Shoesmith, D. & Noël, J. The role of internal cathodic support during the crevice corrosion of Ni-Cr-Mo alloys. *Electrochimica Acta* **283,** 1600–1608. doi:10.1016/j.electacta.2018.07.048 (Sept. 2018).

33. Guo, S., Xu, D., Jiang, G. & Kuang, W. Corrosion behavior and mechanism of Ni-based alloys Hastelloy C2000 and Inconel 740 in chloride-containing supercritical water oxidation. *Journal of Alloys and Compounds* **907,** 164452. doi:10.1016/j.jallcom.2022.164452 (June 2022).

34. Danaee, I., Jafarian, M., Forouzandeh, F., Gobal, F. & Mahjani, M. G. Kinetic Interpretation of a Negative Time Constant Impedance of Glucose Electrooxidation. *The Journal of Physical Chemistry B* **112,** 15933–15940. doi:10.1021/jp8069173 (Dec. 2008).

35. Danaee, I., Jafarian, M., Forouzandeh, F., Gobal, F. & Mahjani, M. Impedance spectroscopy analysis of glucose electro-oxidation on Ni-modified glassy carbon electrode. *Electrochimica Acta* **53,** 6602–6609. doi:10.1016/j.electacta.2008.04.042 (Sept. 2008).

36. Boggs, B. K., King, R. L. & Botte, G. G. Urea electrolysis: Direct hydrogen production from urine. *Chemical Communications,* 4859–4861. doi:10.1039/b905974a (2009).

37. Vedharathinam, V. & Botte, G. G. Understanding the electro-catalytic oxidation mechanism of urea on nickel electrodes in alkaline medium. *Electrochimica Acta* **81,** 292–300. doi:10.1016/j.electacta.2012.07.007 (Oct. 2012).

38. Vedharathinam, V. & Botte, G. G. Direct evidence of the mechanism for the electro-oxidation of urea on Ni(OH)2 catalyst in alkaline medium. *Electrochimica Acta* **108,** 660–665. doi:10.1016/j.electacta.2013.06.137 (Oct. 2013).

39. Wang, J., Mo, F., Fei, J., Ling, W., Cui, M., Lei, H., Jiang, L. & Huang, Y. Insights into the synergistic effect between nickel and molybdenum for catalyzing urea electrooxidation. *Carbon Neutralization* **1,** 267–276. doi:10.1002/cnl2.27 (Dec. 2022).

40. Yang, D., Yang, L., Zhong, L., Yu, X. & Feng, L. Urea electro-oxidation efficiently catalyzed by nickel-molybdenum oxide nanorods. *Electrochimica Acta* **295,** 524–531. doi:10.1016/j.electacta.2018.10.190 (Feb. 2019).

41. Dionigi, F., Zeng, Z., Sinev, I., Merzdorf, T., Deshpande, S., Lopez, M. B., Kunze, S., Zegkinoglou, I., Sarodnik, H., Fan, D., Bergmann, A., Drnec, J., Araujo, J. F. d., Gliech, M., Teschner, D., Zhu, J., Li, W. X., Greeley, J., Roldan Cuenya, B. & Strasser, P. In-situ structure and catalytic mechanism of NiFe and CoFe layered double hydroxides during oxygen evolution. *Nature Communications* **11.** doi:10.1038/s41467-020-16237-1 (Dec. 2020).

42. Steimecke, M., Seiffarth, G. & Bron, M. In Situ Characterization of Ni and Ni/Fe Thin Film Electrodes for Oxygen Evolution in Alkaline Media by a Raman-Coupled Scanning Electrochemical Microscope Setup. *Analytical Chemistry* **89,** 10679–10686. doi:10.1021/acs.analchem.7b01060 (Oct. 2017).

43. Goswami, A., Ghosh, D., Pradhan, D. & Biradha, K. In Situ Grown Mn(II) MOF upon Nickel Foam Acts as a Robust Self-Supporting Bifunctional Electrode for Overall Water Splitting: A Bimetallic Synergistic Collaboration Strategy. *ACS Applied Materials & Interfaces* **14,** 29722–29734. doi:10.1021/acsami.2c04304 (July 2022).

44. Xu, D., Stevens, M. B., Rui, Y., DeLuca, G., Boettcher, S. W., Reichmanis, E., Li, Y., Zhang, Q. & Wang, H. The role of Cr doping in Ni Fe oxide/(oxy)hydroxide electrocatalysts for oxygen evolution. *Electrochimica Acta* **265,** 10–18. doi:10.1016/j.electacta.2018.01.143 (Mar. 2018).

45. Babar, P., Patil, K., Lee, D. M., Karade, V., Gour, K., Pawar, S. & Kim, J. H. Cost-effective and efficient water and urea oxidation catalysis using nickel-iron oxyhydroxide nanosheets

synthesized by an ultrafast method. *Journal of Colloid and Interface Science* **584,** 760–769. doi:10.1016/j.jcis.2020.09.108 (Feb. 2021).

46. Feng, K., Tian, J., Guo, M., Wang, Y., Wang, S., Wu, Z., Zhang, J., He, L. & Yan, B. Experimentally unveiling the origin of tunable selectivity for CO_2 hydrogenation over Ni-based catalysts. *Applied Catalysis B: Environmental* **292,** 120191. doi:10.1016/j.apcatb.2021.120191 (Sept. 2021).

47. Yan, X., Zhang, W.-D., Xu, H., Xiang, L., Liu, J., Yang, J., Zhu, H. & Gu, Z.-G. Hierarchical NiCr hydroxide nanospheres with tunable domain boundaries for highly efficient urea electro-oxidation. *Electrochimica Acta* **388,** 138633. doi:10.1016/j.electacta.2021.138633 (Aug. 2021).

48. Conrad, H., Corbett, J. & Golden, T. D. Electrochemical Deposition of γ-Phase Zinc-Nickel Alloys from Alkaline Solution. *ECS Transactions* **33,** 85–95. doi:10.1149/1.3566091 (Mar. 2011).

49. Lu, S., Pan, J., Huang, A., Zhuang, L. & Lu, J. Alkaline polymer electrolyte fuel cells completely free from noble metal catalysts. doi:10.1073/pnas.0810041106 (2008).

50. Ge, J., Lai, Y., Guan, M., Xiao, Y., Kuang, J. & Yang, C. Nickel borate with a 3D hierarchical structure as a robust and efficient electrocatalyst for urea oxidation. *Environmental Science: Nano* **8,** 1326–1335. doi:10.1039/d0en01247e (5 May 2021).

51. Periyasamy, S., Subramanian, P., Levi, E., Aurbach, D., Gedanken, A. & Schechter, A. Exceptionally Active and Stable Spinel Nickel Manganese Oxide Electrocatalysts for Urea Oxidation Reaction. *ACS Applied Materials & Interfaces* **8,** 12176–12185. doi:10.1021/acsami.6b02491 (19 May 2016).

52. Annan, K. Mathematical modeling of the dynamic exchange of solutes during bicarbonate dialysis. *Mathematical and Computer Modelling* **55,** 1691–1704. doi:10.1016/j.mcm.2011.11.013 (5-6 Mar. 2012).

53. Yaqoob, T., Ahsan, M., Farrukh, S. & Ahmad, I. Design and Development of a Computational Tool for a Dialyzer by Using Computational Fluid Dynamic (CFD) Model. *Membranes* **11,** 916. doi:10.3390/membranes11120916 (12 Nov. 2021).

54. Gheriany, I. E., Abdel-Aziz, M. H., El-Ashtoukhy, E.-S. Z. & Sedahmed, G. H. Electrochemical removal of urea from wastewater by anodic oxidation using a new cell design: An experimental and modeling study. *Process Safety and Environmental Protection* **159,** 133–145. doi:10.1016/j.psep.2021.12.055 (Mar. 2022).

55. Klaus, S., Cai, Y., Louie, M. W., Trotochaud, L. & Bell, A. T. Effects of Fe Electrolyte Impurities on Ni(OH) ₂ /NiOOH Structure and Oxygen Evolution Activity. *The Journal of Physical Chemistry C* **119,** 7243–7254. doi:10.1021/acs.jpcc.5b00105 (Apr. 2015).

56. Trotochaud, L., Young, S. L., Ranney, J. K. & Boettcher, S. W. Nickel–Iron Oxyhydroxide Oxygen-Evolution Electrocatalysts: The Role of Intentional and Incidental Iron Incorporation. *Journal of the American Chemical Society* **136,** 6744–6753. doi:10.1021/ja502379c (May 2014).

57. Macdougall, I. C. Supplemental iron via dialysate: a novel mode of delivery for hemodialysis patients. *Kidney International* **88,** 946–949. doi:10.1038/ki.2015.260 (5 Nov. 2015).

58. Marino, M., Misuri, L. & Brogioli, D. A new open source software for the calculation of the liquid junction potential between two solutions according to the stationary Nernst-Planck equation. doi:10.48550/arXiv.1403.3640 (Mar. 2014).

59. Tang, Y., Liu, Y., Yu, S., Zhao, Y., Mu, S. & Gao, F. Hydrothermal synthesis of a flower-like nano-nickel hydroxide for high performance supercapacitors. *Electrochimica Acta* **123,** 158–166. doi:10.1016/j.electacta.2013.12.187 (Mar. 2014).

60. McCrory, C. C. L., Jung, S., Peters, J. C. & Jaramillo, T. F. Benchmarking Heterogeneous Electrocatalysts for the Oxygen Evolution Reaction. *Journal of the American Chemical Society* **135,** 16977–16987. doi:10.1021/ja407115p (Nov. 2013).

61. Chakthranont, P., Kibsgaard, J., Gallo, A., Park, J., Mitani, M., Sokaras, D., Kroll, T., Sinclair, R., Mogensen, M. B. & Jaramillo, T. F. Effects of Gold Substrates on the Intrinsic and Extrinsic Activity of High-Loading Nickel-Based Oxyhydroxide Oxygen Evolution Catalysts. *ACS Catalysis* **7,** 5399–5409. doi:10.1021/acscatal.7b01070 (Aug. 2017).

62. Ouseph, R. & Ward, R. A. Increasing Dialysate Flow Rate Increases Dialyzer Urea Mass Transfer-Area Coefficients During Clinical Use. *American Journal of Kidney Diseases* **37,** 316–320. doi:10.1053/ajkd.2001.21296 (Feb. 2001).

63. Gostoli, C. & Gatta, A. Mass transfer in a hollow fiber dialyzer. *Journal of Membrane Science* **6,** 133–148. doi:10.1016/S0376-7388(00)82156-0 (Jan. 1980).

64. Locatelli, F., Altieri, P., Andrulli, S., Bolasco, P., Sau, G., Pedrini, L. A., Basile, C., David, S., Feriani, M., Montagna, G., Di Iorio, B. R., Memoli, B., Cravero, R., Battaglia, G. & Zoccali, C. Hemofiltration and Hemodiafiltration Reduce Intradialytic Hypotension in ESRD. *Journal of the American Society of Nephrology* **21,** 1798–1807. doi:10.1681/ASN.2010030280 (Oct. 2010).

65. Kirsch, A. H., Lyko, R., Nilsson, L.-G., Beck, W., Amdahl, M., Lechner, P., Schneider, A., Wanner, C., Rosenkranz, A. R. & Krieter, D. H. Performance of hemodialysis with novel medium cut-off dialyzers. *Nephrology Dialysis Transplantation,* gfw310. doi:10.1093/ndt/gfw310 (Sept. 2016).

66. Leypoldt, J. K., Cheung, A. K., Agodoa, L. Y., Daugirdas, J. T., Greene, T., Keshaviah, P. R. & Beck, G. J. Hemodialyzer mass transfer-area coefficients for urea increase at high dialysate flow rates. *Kidney International* **51,** 2013–2017. doi:10.1038/ki.1997.274 (June 1997).

67. Benziger, J., Chia, E., Karnas, E., Moxley, J., Teuscher, C. & Kevrekidis, I. G. The stirred tank reactor polymer electrolyte membrane fuel cell. *AIChE Journal* **50,** 1889–1900. doi:10.1002/aic.10158 (Aug. 2004).

68. Small, L. J., Pratt, H. D. & Anderson, T. M. Crossover in Membranes for Aqueous Soluble Organic Redox Flow Batteries. *Journal of The Electrochemical Society* **166,** A2536–A2542. doi:10.1149/2.0681912jes (July 2019).

69. Rommerskirchen, A., Roth, H., Linnartz, C. J., Egidi, F., Kneppeck, C., Roghmans, F. & Wessling, M. Mitigating Water Crossover by Crosslinked Coating of Cation-Exchange Membranes for Brine Concentration. *Advanced Materials Technologies* **6,** 2100202. doi:10.1002/admt.202100202 (Oct. 2021).

70. Eriksson, B., Grimler, H., Carlson, A., Ekström, H., Wreland Lindström, R., Lindbergh, G. & Lagergren, C. Quantifying water transport in anion exchange membrane fuel cells. *International Journal of Hydrogen Energy* **44,** 4930–4939. doi:10.1016/j.ijhydene.2018.12.185 (Feb. 2019).

71. Wang, X.-x., Fu, H., Du, D.-m., Zhou, Z.-y., Zhang, A.-g., Su, C.-f. & Ma, K.-s. The comparison of pKa determination between carbonic acid and formic acid and its application to prediction of the hydration numbers. *Chemical Physics Letters* **460,** 339–342. doi:10.1016/j.cplett.2008.05.074 (July 2008).

72. Goldstein, S. L., Allsteadt, A., Beck, W. & Nilsson, L.-G. Evaluation of the Polyflux® 6H Dialyzer in Pediatric Patients Receiving Maintenance Hemodialysis. *The International Journal of Artificial Organs* **30,** 321–324. doi:10.1177/039139880703000407 (Apr. 2007).

73. Al-Biltagi, M., Tolba, O. A., ElHafez, M. A. A., Abo-Elezz, A. A. E., EL Kady, E. K. & Hazza, S. M. E.-d. Oxidative stress and cardiac dysfunction in children with chronic renal failure on regular hemodialysis. *Pediatric Nephrology* **31,** 1329–1339. doi:10.1007/s00467-016-3314-8 (Aug. 2016).

74. Soo, E. & Schaefer, F. in *Handbook of Dialysis Therapy* 948–954 (Elsevier, 2017). doi:10.1016/B978-0-323-39154-2.00082-5.

75. Liu, L., Zhou, Z. & Peng, C. Sonochemical intercalation synthesis of nano γ-nickel oxyhydroxide: Structure and electrochemical properties. *Electrochimica Acta* **54,** 434–441. doi:10.1016/j.electacta.2008.07.055 (Dec. 2008).

76. Jadhav, R. G. & Das, A. K. Pulse electrodeposited, morphology controlled organic–inorganic nanohybrids as bifunctional electrocatalysts for urea oxidation. *Nanoscale* **12,** 23596–23606. doi:10.1039/D0NR07236B (2020).

77. Xu, Q., Yu, T., Chen, J., Qian, G., Song, H., Luo, L., Chen, Y., Liu, T., Wang, Y. & Yin, S. Coupling Interface Constructions of $FeNi_3$-MoO_2 Heterostructures for Efficient Urea Oxidation and Hydrogen Evolution Reaction. *ACS Applied Materials & Interfaces* **13,** 16355–16363. doi:10.1021/acsami.1c01188 (Apr. 2021).

78. Anuratha, K. S., Rinawati, M., Wu, T.-H., Yeh, M.-H. & Lin, J.-Y. Recent Development of Nickel-Based Electrocatalysts for Urea Electrolysis in Alkaline Solution. *Nanomaterials* **12,** 2970. doi:10.3390/nano12172970 (Aug. 2022).